A&A 663, A136 (2022)
https://doi.org/10.1051/0004-6361/202243312

Astronomy & Astrophysics

Enhanced reactivity of oxygen-functionalised PAHs with atomic hydrogen – A route to the formation of small oxygen-carrying molecules

R. Jaganathan[1], F. D. S. Simonsen[1], J. D. Thrower[1], and L. Hornekær[1,2]

[1] Center for Interstellar Catalysis (InterCat), Department of Physics and Astronomy, Aarhus University, Ny Munkegade 120, Aarhus C 8000, Denmark
[2] Interdisciplinary Nano-Science Centre (iNano), Aarhus University, Gustav Wieds Vej 14, Aarhus C 8000, Denmark
e-mail: liv@phys.au.dk

Received 11 February 2022 / Accepted 4 June 2022

ABSTRACT

Aims. We investigate the interaction of a linear, catacondensed polycyclic aromatic hydrocarbon (PAH), pentacene ($C_{22}H_{14}$), and its oxygen-functionalised form 6, 13 pentacenequinone ($C_{22}H_{12}O_2$) with atomic hydrogen (H) under interstellar conditions. We compare their reaction cross-sections and reaction products to elucidate the possible role played by oxygen-functionalised PAHs in the formation of small oxygen-carrying molecules in the interstellar medium.
Methods. We present temperature-programmed desorption measurements in combination with mass spectrometry. The evolution of the mass distribution of the desorbed species with increasing H-atom fluence and their peak desorption temperatures give insight into the reaction products.
Results. The experiments reveal reaction cross-sections that are significantly larger for the oxygen-functionalised species compared to pentacene. For both pentacene and 6, 13 pentacenequinone, hydrogenated species with an even number of excess H-atoms dominate over hydrogenated species with an odd number of H-atoms. The end product, after exposure to large H-atom fluences, for both pentacene and PQ is fully superhydrogenated pentacene ($C_{22}H_{36}$), with little evidence for any remaining oxygen-containing species. This suggests the release of small molecules such as OH and/or H_2O by the abstraction of oxygen atoms during hydrogenation, indicating that oxygen-functionalised PAHs can enable the formation of small oxygen-bearing molecules under interstellar conditions.

Key words. astrochemistry – molecular processes – methods: laboratory: molecular – methods: laboratory: solid state – ISM: molecules

1. Introduction

Polycyclic aromatic hydrocarbons (PAHs) are widely acknowledged as the carriers of a family of infrared (IR) emission bands with typical emission features located between 3 and 20 μm, seen in the IR spectra of almost all interstellar objects, ranging from planetary nebulae to HII regions (Tielens 2008). The observed spectral features are attributed to a mixture of ionised and neutral, functionalised, or substituted PAHs of different sizes (Salama 2008). PAHs account for up to 15% of the cosmic carbon budget and play an important role in the physics and chemistry of the interstellar medium (ISM) (Tielens 2005; Peeters et al. 2021). The role of PAHs in ISM chemistry has been recognised in the context of (i) H_2 formation (Habart et al. 2004; Rauls & Hornekær 2008; Le Page et al. 2009; Mennella et al. 2011; Thrower et al. 2012); (ii) the top-down formation of fullerenes (Berné & Tielens 2012; Zhen et al. 2014); (iii) photo-dissociation, leading to small hydrocarbons (Pety et al. 2005); and (iv) precursors of prebiotic molecules via a top-down mechanism (Allamandola 2011; Mattioda et al. 2020).

During their lifetime in the ISM, PAHs can be both functionalised with chemical side groups, such as -H, -OH, =O, and -C_xH_y, and/or be substituted with heteroatoms, mainly nitrogen and oxygen in the carbon skeleton. Such functionalisation, in certain cases, results in a dipole moment that carries the potential for detection in the radio and microwave spectral regions. The discovery of the aromatic CN-functionalised molecules, benzonitrile ($C_6H_5(CN)$) and 1-cyanonaphthalene (1-$C_{10}H_7(CN)$) (McGuire et al. 2018, 2021), and a PAH with a five-membered ring, indene (C_9H_8) (Burkhardt et al. 2021; Cernicharo et al. 2021), promises the detection of PAHs with a dipole moment such as the curved PAH corannulene, nitrogen- or oxygen-substituted heterocyclic PAHs, and oxygen-functionalised PAHs among others.

The presence of superhydrogenated (H-functionalised) and methylated PAHs is suggested by observations of a spatial correlation between aliphatic C-H stretching and aromatic C-H and C-C vibrations (Joblin et al. 1996; Bernstein et al. 1996; Sloan et al. 1997), while Peeters et al. (2002) attribute the 6.0 μm emission feature observed in the ISO spectrum of the Red Rectangle to the C=O stretch of PAH quinones. Density functional theory (DFT) calculations by Sadjadi et al. (2015) suggest that the 11.3 μm IR band is likely due to substituted PAHs, including oxygen-containing species.

In cold regions of the ISM, PAHs are expected to be frozen out on dust grains. Laboratory experiments investigating the processing of water-ice and PAH mixtures by energetic radiation such as UV light, electrons, or protons show that superhydrogenated PAHs are produced, alongside PAHs with alcohol and ketone functional groups indicating that such oxygen-bearing PAH species could be formed in the ISM on icy grains (Bernstein et al. 1999; Gudipati & Yang 2012; Bouwman et al. 2011;

Guennoun et al. 2011a,b; Noble et al. 2020). Cook et al. (2015) estimate that interstellar ices could contain neutral and ionised PAHs, alcohols, ketones, and quinones at the 2–4% level relative to water. The products of PAH processing in interstellar ices may also form a part of the material forming asteroids and comets and hence may play a role in astrobiological processes as many important biological molecules contain functionalised aromatic rings. Dulieu et al. (2019) studied the interaction of coronene and superhydrogenated coronene with oxygen atoms and show that the oxygenation of coronene is more effective than hydrogenation, and it leads to significant fragmentation. Chen et al. (2017) show that the oxygen-functionalised PAH, bisanthenquinone ($C_{28}H_{12}O_2$) cation, is not photo-stable and preferentially loses neutral CO units via photo-fragmentation. Hence, the presence of oxygen-functionalised PAHs in interstellar space is still debated.

The interaction of the pericondensed PAH coronene with atomic hydrogen (H) and deuterium has been studied both theoretically and experimentally (Rauls & Hornekær 2008; Thrower et al. 2012; Mennella et al. 2011, 2021; Cazaux et al. 2016; Jensen et al. 2019). These studies reveal the catalytic role of superhydrogenated PAHs in H_2 formation, which could be an important process in photodissociation regions where H_2 formation rates cannot be explained by grain-surface reactions alone (Wakelam et al. 2017; Habart et al. 2004). Pentacene ($C_{22}H_{14}$) is a linear catacondensed PAH and is an important member of a family of linear PAHs termed acenes (Knipp et al. 2003). They are characterised by zigzag edges that have a strong C-H out-of-plane bending mode, thereby contributing to the observed 11.2 μm feature (Candian & Sarre 2015). Theoretical calculations have revealed that the hydrogenation sequence is dependent on the structure of the PAH, with zigzag edges being more reactive towards H-atoms (Campisi et al. 2020; Rasmussen 2013; Rauls & Hornekær 2008; Jensen et al. 2019; Cazaux et al. 2019), thereby potentially having an important role in interstellar chemistry. In addition, the presence of different functional groups on the pristine PAH skeleton also influences the reactivity towards atomic hydrogen (and other species) and might lead to a small molecule formation through abstraction reactions, similar to the observed H_2 formation from superhydrogenated PAHs (Mennella et al. 2011; Thrower et al. 2012).

In this paper we study, experimentally, the interaction of neutral 6, 13–pentacenequinone (PQ) and pentacene with H-atoms and compare their reactivity and reaction products using temperature-programmed desorption (TPD) combined with quadrupole mass spectrometry (QMS). We note that PQ ($C_{22}H_{12}O_2$) is an oxygen-functionalised pentacene analogue, where two oxygen atoms are attached as ketone groups to opposing carbon atoms in the central ring. The possible hydrogenation sequence and the presence of certain stable superhydrogenated species for pentacene are explained in Campisi et al. (2020), while in this work the reaction cross-section for the first H-atom addition is presented in order to shed light on the reactivity of the zigzag edge. The hydrogenation sequence and the reaction cross-section for PQ is presented and compared to that of pentacene to demonstrate the effect of the oxygen-functional group on the interaction of PAHs with H-atoms.

2. Experimental details

Thermal desorption experiments were performed under ultra-high vacuum (UHV) conditions in a chamber with a typical base pressure of 1×10^{-10} mbar. A home-built Knudsen cell-type thermal evaporator was used to deposit 6, 13–pentacenequinone ($C_{22}H_{12}O_2$)(PQ) (>95% from TCI Europe) and pentacene (>99.995% from Sigma-Aldrich)($C_{22}H_{14}$) onto a clean, highly oriented pyrolytic graphite (HOPG) surface kept at 290 ± 5 K. Panels i and iii in Fig. 1 show the molecular structures of these species. The source was degassed thoroughly prior to deposition in order to remove any residual contaminants. The HOPG substrate was cleaved with adhesive tape before mounting on a Tantalum (Ta) plate attached to a water-cooled sample holder which was then mounted in the UHV chamber. The temperature of the sample was measured with a type-C thermocouple secured between the front face of the substrate and the Ta plate. A pyrometer was used to calibrate the temperature using the emissivity of graphite (0.85). Prior to each measurement, the HOPG was annealed to 1100 K in UHV to remove any contaminants.

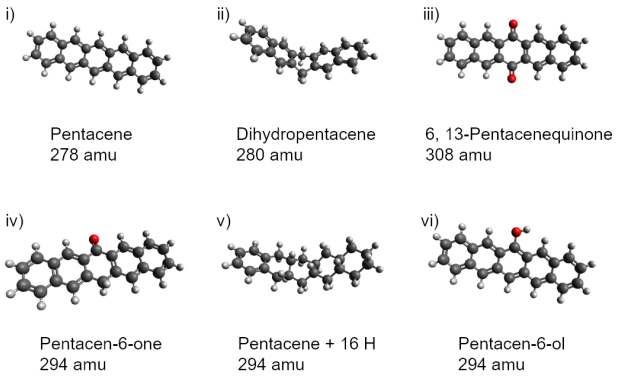

Fig. 1. Molecular structures of the species referred to in the article with their corresponding masses. The structure for Pentacene with 16H is representative.

A monolayer of pentacene was consistently produced by exposing the clean HOPG surface to the source operated at 403 K for 2 min, followed by annealing the surface to 330 K for 5 min to desorb the multi-layers. For PQ, a monolayer of molecules could be prepared by exposing the clean HOPG surface to the source operated at 443 K for 2 min, followed by annealing the surface to 380 K for a second.

The pentacene and PQ monolayers were exposed to H-atoms from a hydrogen atom beam source (HABS) (Tschersich & Von Bonin 1998; Tschersich 2000; Tschersich et al. 2008). The HABS was operated at ≈2200 K to dissociate H_2 (99.99%, Linde). The atoms produced were subsequently cooled collisionally by passing them through a curved quartz nozzle attached to HABS. The shape of the nozzle ensures at least four collisions between the hot H-atoms and the inner surface of the nozzle. Ioppolo et al. (2013) used a similar cooling setup and argue that it resulted in cooling the H-atoms to 300 K. Further, inelastic collision simulations incorporating the hard cube scattering model (Grimmelmann et al. 1980) estimated the H-atom beam temperature to be ≈1500 K (Simonsen 2020). This estimate should be viewed as a strict upper limit as the simulations do not take further cooling effects into account such as collisions with lighter surface elements other than those assumed in the simulation or trapping-desorption (Fan & Manson 2009). Hence, we assume 300 K $\leq T_{\mathrm{H\ atoms}} <$ 1500 K. The H-atom flux was estimated to be $(6 \pm 3) \times 10^{14}$ atoms cm^{-2} s^{-1} through calibration measurements of atomic H uptake and exchange with D-atoms on a reconstructed Si(100)–(2×1) surface (Simonsen 2020).

Temperature-programmed desorption measurements were performed by heating the sample at a rate of 1 Ks^{-1} with the

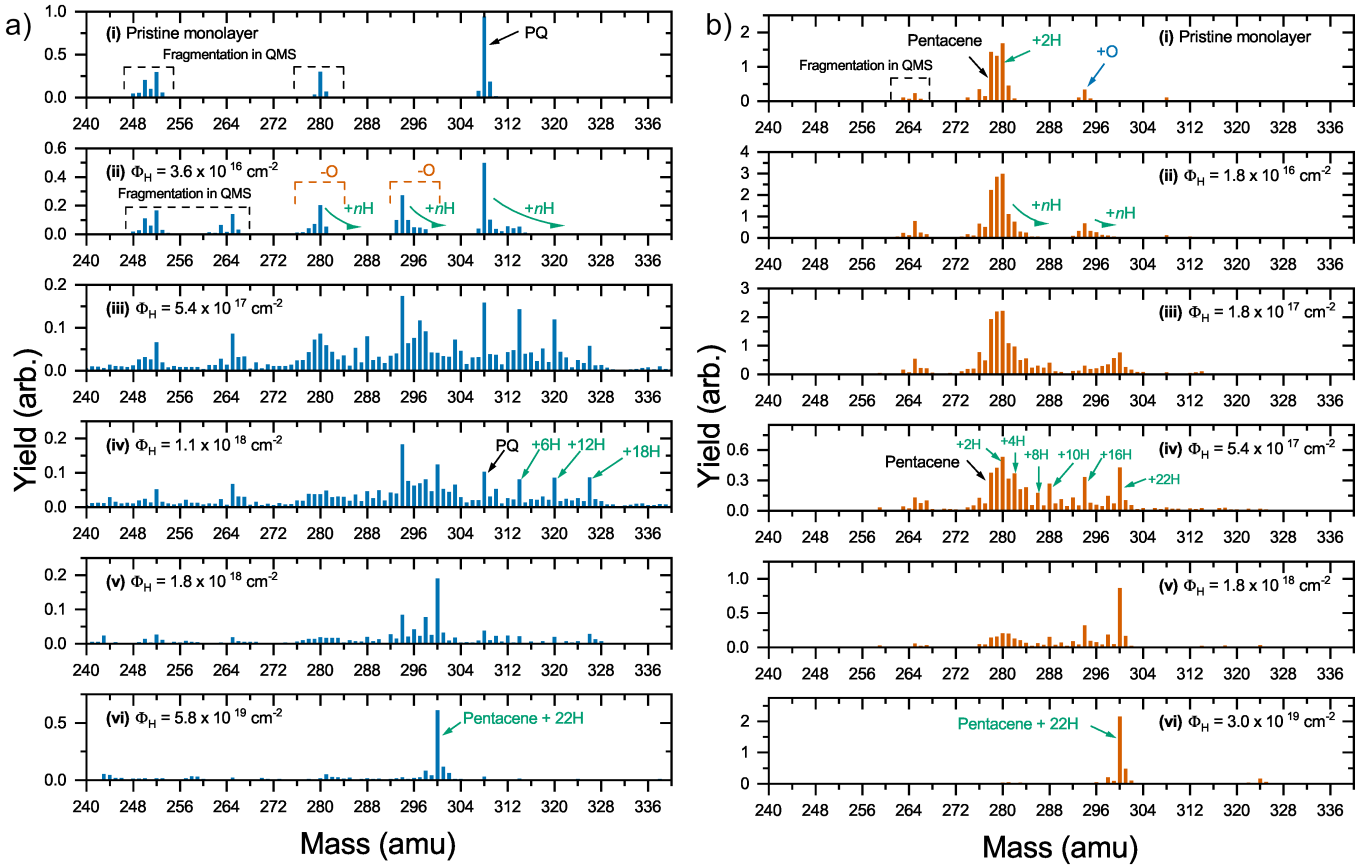

Fig. 2. Desorption product mass distributions obtained following exposure of a monolayer of (*a*) PQ and (*b*) pentacene to increasing H-atom fluences. (*a*)(i) The mass distribution of the monolayer of PQ (m/z = 308). (*a*)(ii)–(vi) Mass distributions extending to masses lower and higher than the pristine PQ indicating abstraction and addition reactions, eventually reaching mass 300 which is a fully superhydrogenated pentacene. (*b*)(i) The mass distribution of the monolayer of pentacene (m/z = 278) with the prominent contaminants dihydropentacene (m/z = 280) and oxygenated pentacene species with m/z = 294 and 308. (*b*)(ii)–(vi) Mass distributions shifting towards higher masses with increasing H-atom exposure intervals, eventually reaching m/z = 300 corresponding to fully superhydrogenated pentacene.

aid of a PID controller (Lakeshore Model 340) and the desorbing species were detected with a quadrupole mass spectrometer (QMS; Extrel CMS LLC), which can detect species with a mass-to-charge ratio (m/z) of up to 500. In our experiments, z = 1 and hence m/z is equal to the mass of the species. The TPD trace for each mass in the range of interest (m/z = 240–340) was integrated over the desorption timescale to obtain the mass spectrum. The absolute yield of the parent molecule was used to calculate the reaction cross-section.

3. Results and discussion

The product mass distributions obtained after exposing a monolayer of PQ and that of pentacene to an increasing fluence of H-atoms are presented in Figs. 2a and b, respectively. Figure 2a i shows the mass distribution of the desorption products for the pristine PQ monolayer in which the prominent mass peaks seen are m/z = 308 (PQ), 280, and 252. As expected, the yield of PQ, having m/z = 308, is the highest peak, while the smaller peaks in the range m/z = 306–310 can be attributed to H loss in the QMS and the natural abundance of ^{13}C. The peaks at m/z = 252 and 280 are the dominant fragments of PQ that formed in the QMS and could correspond to the loss of CO or C_2H_4 species (Linstrom & Mallard 2021). The mass distribution of the pristine pentacene monolayer, Fig. 2b i, shows several prominent peaks – pentacene (m/z = 278), along with the contaminants dihydropentacene (m/z = 280) and the oxygen-containing species (m/z = 294 and 308) (Roberson et al. 2005; Jurchescu et al. 2004; De Angelis et al. 2009; Campisi et al. 2020). Readers can refer to Fig. 1 to see the structures.

Panels b ii–vi in Fig. 2 show the mass distributions of the desorption products when the pristine pentacene monolayer is exposed to increasing H-atom fluences. As the H-atom fluence increases, there is an increase in the yield of masses greater than m/z = 278, which corresponds to the formation of superhydrogenated pentacene molecules. Figure 2b iv shows the mass distribution corresponding to a H-atom fluence of 5.4×10^{17} cm^{-2} in which specific hydrogenation states of pentacene with 2, 4, 6, 10, 16, and 22 extra H-atoms appear more abundant than the others. The prominence of these species and the associated hydrogenation sequence is related to the presence of energetic barriers in the hydrogenation sequence, as shown in Campisi et al. (2020). The mass distribution for the very long H-atom exposure (Fig. 2b vi) is dominated by a single peak at m/z = 300, corresponding to fully superhydrogenated pentacene ($C_{22}H_{36}$) with one H-atom added to every carbon atom, thereby indicating that H-atom addition reactions dominate over H-atom abstraction for superhydrogenated pentacene species. Also seen are masses due to H loss in the QMS and those due to the natural abundance of ^{13}C.

Panels a ii–vi in Fig. 2 show the mass distribution of the desorption products when the pristine PQ monolayer is exposed to

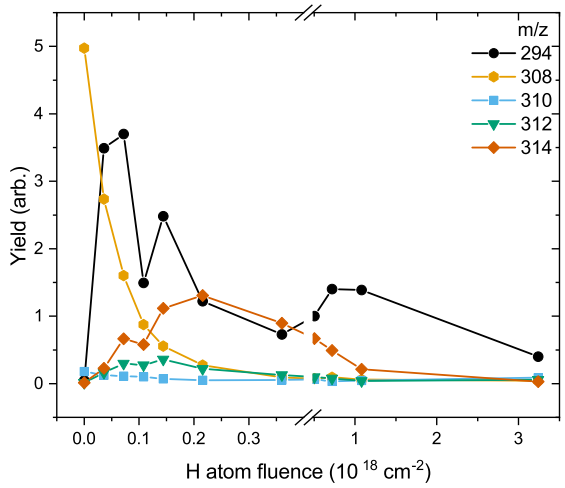

Fig. 3. Total yield of the pristine PQ ($m/z = 308$), an abstraction product ($m/z = 294$), and the superhydrogenated products ($m/z = 310$, 312, and 314) as a function of H-atom fluence. The yield of pristine PQ reduces with increasing exposure to H fluence. The superhydrogenated product with $m/z = 314$ peaks only at an intermediate H exposure. The product of abstraction, $m/z = 294$, dominates the mass distribution for exposure to lower H fluences and again at an exposure to high H-atom fluences.

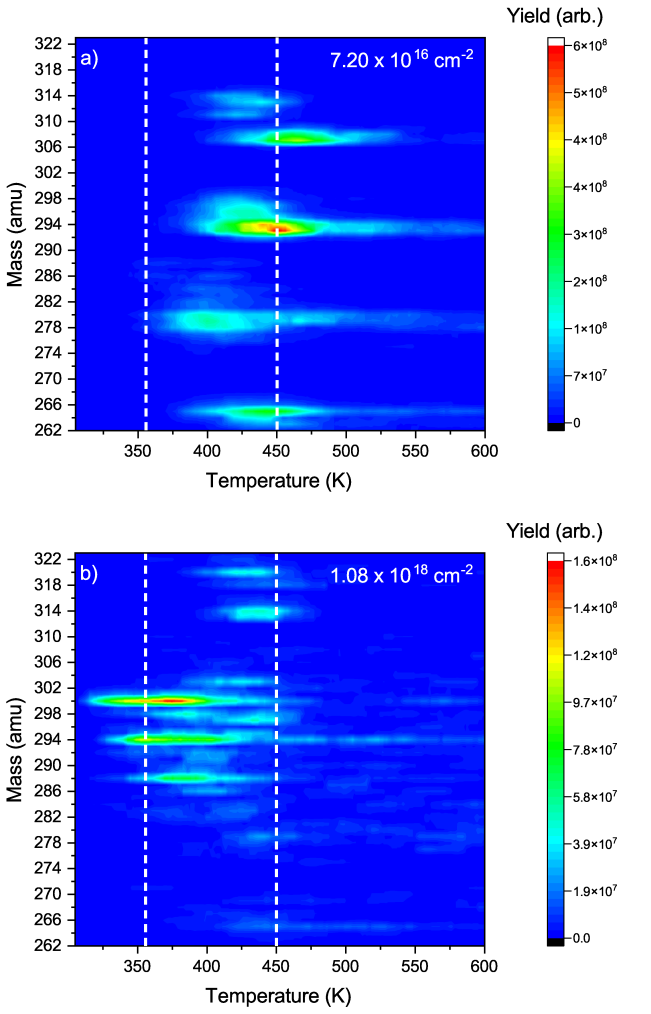

Fig. 4. Contour plots corresponding to the exposure of the PQ monolayer to (*a*) a low fluence showing $m/z = 294$ desorbing at circa 450 K and (*b*) a higher fluence wherein $m/z = 294$ desorbs at circa 350 K.

increasing H-atom fluences. It is observed that there is a reduction in the yield of PQ, as shown in Fig. 2a, accompanied by an increase in the yield of masses both greater than and less than $m/z = 308$ (Figs. 2a ii–vi). The observation of masses greater than $m/z = 308$ is consistent with the formation of superhydrogenated PQ molecules, that is to say the addition of H-atoms to PQ. Masses below 308 amu, in particular masses $m/z = 294$ and 280, are ascribed to abstraction of oxygen atom(s) followed or preceded by the addition of H-atoms. Fragments centred around $m/z = 265$ also appear and it is likely that they formed by fragmentation of the product with $m/z = 294$ in the QMS. The fragment with $m/z = 265$ is also seen in the mass distribution of the pentacene monolayer, Fig. 2b i, where the species with $m/z = 294$ amu is present as a contaminant.

In considering the mass distribution shown in Fig. 2a iv, the superhydrogenated products with $m/z = 314$, 320, and 326 (marked with arrows) corresponding to the addition of 6, 12, and 18 H-atoms to PQ have prominent peaks, implying their relative stability and hence suggesting a barrier to the further addition of H-atoms. The mass difference between the species is 6 amu, corresponding to the addition of extra H-atoms to a complete aromatic ring and the barrier could be related to breaking the aromaticity of the next ring under attack. In Jensen et al. (2019) and Campisi et al. (2020), certain stable masses of superhydrogenated coronene and pentacene are similarly explained by using the concept of residual aromaticity, whereby a barrier to the further addition of H-atoms to the molecule is due to the next addition leading to a loss of an aromatic ring. The stable species with 6, 12, and 18 extra H-atoms when compared to the stable species for pentacene (4, 10, and 16 extra H-atoms) show a difference of two H-atoms. This can be attributed to the addition of H-atoms to both the oxygen and the carbon atoms of the ketone groups on the central ring.

For the exposure of the PQ monolayer to the highest H-atom fluence, which corresponds to the steady state of the system, the distribution is dominated by the product having $m/z = 300$ amu, which is identified as fully superhydrogenated pentacene ($C_{22}H_{36}$) and the same as that observed for pentacene when exposed to the highest H-atom fluences (Figs. 2a vi and b vi). However, fully superhydrogenated PQ, that is to say PQ with 22 extra H-atoms having $m/z = 330$, is not seen even for exposures to the highest H-atom fluence. In fact, none of the superhydrogenated PQ species survive at the higher H fluences, indicating that the PQ molecule easily loses the oxygen atoms possibly releasing OH, H_2O, or CHO.

Figure 3 shows the evolution of the yield of $m/z = 294$, 308, 310, 312, and 314 with increasing H-atom fluence. At low fluences, the product of abstraction, $m/z = 294$, dominates the mass distribution, while the superhydrogenated products with 2 and 4 additional H-atoms contribute only a small fraction of the total yield. As mentioned, the yield of pristine PQ decreases rapidly with increasing H-atom fluence. The superhydrogenated product with $m/z = 314$, corresponding to the addition of 6 H-atoms, is observed to increase only at intermediate fluences after the major initial drop in the yield of the PQ peak at $m/z = 308$. This indicates that abstraction of the oxygen atom from PQ dominates the reaction, rather than the addition of H-atoms. At the exposure to high H-atom fluences, $m/z = 294$ dominates again indicating that a mixture of species contribute to the $m/z = 294$ yield.

More insight can be gained as to the nature of the species contributing to $m/z = 294$ by considering the desorption

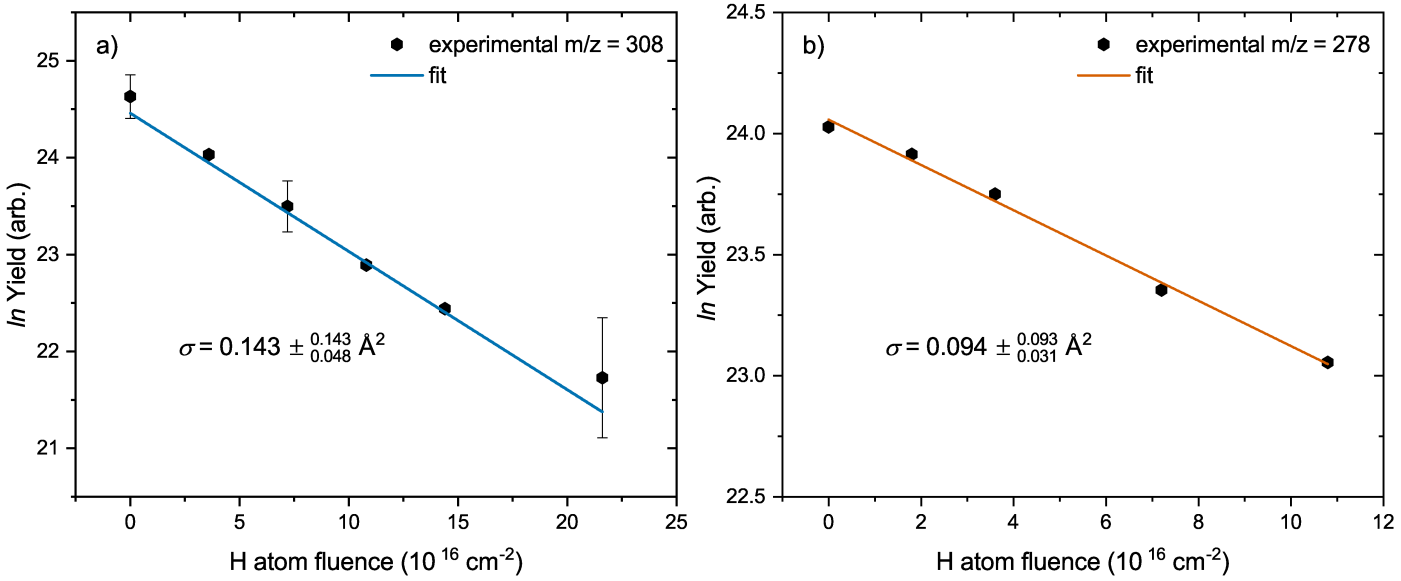

Fig. 5. Natural logarithm (ln) of the experimentally derived yield of (a) $m/z = 308$ (pristine PQ) and (b) $m/z = 278$ (pristine pentacene) as a function of H-atom fluence (dots). The solid curves represent the best linear fit from which the cross-section was obtained.

temperatures of the species contributing to the signal at m/z = 294 at low and at high fluences. Panels a and b in Fig. 4 show the contour plots for the exposure of the PQ monolayer to two different H-atom fluences – a low H fluence of 7.20×10^{16} cm^{-2} and a higher fluence of 1.08×10^{18} cm^{-2} for a selected mass range. The peak desorption rate in m/z = 294 is observed to occur at circa 450 K following exposure to low H-atom fluence, while it is observed to decrease to circa 350 K following the exposure to higher H-atom fluence, indicating decreased binding to the substrate of the species that formed following exposure to a higher H-atom fluence. Thrower et al. (2012), Skov et al. (2016), and Jensen et al. (2019) observed that superdeuterated and superhydrogenated coronene species leave the surface at a lower temperature than the parent molecule. A similar behaviour can be expected for superhydrogenated pentacene species indicating that the dominant product having m/z = 294 formed following exposure to higher fluence is the superhydrogenated pentacene species ($C_{22}H_{30}$), as shown in Fig. 1 v. This species corresponds to the addition of 16 H-atoms to pentacene, implying that the parent PQ molecule has lost both oxygen-atoms. Following exposure to the lower H fluence, m/z = 294 is expected to be dominated by products corresponding to the loss of one oxygen atom from PQ and the subsequent addition of two H-atoms. This could result in either pentacene with a single ketone group on the centre ring (pentacen-6-one) or pentacene with an alcohol group on the centre ring (pentacen-6-ol), both of these molecules are illustrated in Figs. 1 iv and vi. Additionally, in Fig. 4a, the species with m/z = 265 is also seen to desorb at the same temperature as m/z = 294 and hence the species with m/z = 265 can be considered a fragment of the oxygen-containing product with m/z = 294 in the QMS corresponding to the loss of HCO. The species with m/z = 265 is not observed to have the same desorption temperature as the superhydrogenated pentacene product with m/z = 294 which dominates at the exposure to high H-atom fluences (Fig. 4b). Thus, the exposure of PQ to H-atoms leads to the abstraction of oxygen atoms from the molecule and the potential formation of small oxygen-containing species such as OH and HCO.

From the decay in the yield of the parent PAH, one can obtain the cross-section for the reaction of a H-atom with the PAH molecule using the following first order rate equation:

$$I_{m_p}(\Phi_H) = I_0 \exp(-\sigma \times \Phi_H) + I_\infty, \quad (1)$$

where I_{m_p} is the yield of the pristine PAH corresponding to the exposure to a certain fluence Φ_H, m_p refers to the parent mass, that is to say m_p = 308 for PQ and m_p = 278 for pentacene, I_0 is the yield of the pristine PAH without exposure to H, σ is the reaction cross-section for a H-atom with the pristine PAH molecule, Φ_H is given by the flux multiplied by the time interval, and I_∞ is the residual signal at infinite time.

Panels a and b in Fig. 5 show the natural logarithm of the yield of m/z = 308 and 278 plotted against the fluence of the H-atoms for PQ and pentacene, respectively. The slope of the linear fit gives $\sigma_1 = 0.143\ (^{+0.143}_{-0.048})$ Å^2 as the reaction cross-section for a PQ molecule. For pentacene, $\sigma = 0.094\ (^{+0.093}_{-0.031})$ Å^2. It should be noted that the reaction cross-section is a combination of H-atom addition and H-atom (and oxygen atom for PQ) abstraction cross-sections.

The reaction cross-section for pentacene is larger than that of coronene, $\sigma = 0.027\ (^{+0.027}_{-0.009})$ Å^2, as obtained by Jensen et al. (2019), providing experimental evidence for the higher reactivity of zigzag edges as found theoretically by Campisi et al. (2020). The reaction cross-section of PQ is a factor of 1.5 larger than that of pentacene, indicating that the presence of oxygen-functional groups in a PAH enhances its reactivity towards H-atoms. This increased reactivity is expected to result in the formation of small oxygen-carrying molecules via oxygen atom abstraction reactions.

4. Conclusion

The presented results demonstrate that a H-atom exposure of pentacene and 6, 13–pentacenequinone (PQ) leads to both addition and abstraction reactions. For both pentacene and its oxygen-functionalised form, a prolonged H-atom exposure leads to the formation of fully superhydrogenated pentacene ($C_{22}H_{36}$). This implies that for PQ, H addition leads to the loss of the oxygen-functional groups via the formation of small

oxygen-containing species such as OH. Certain superhydrogenated species with an even number of additional H-atoms have increased stability and may therefore be more prominent superhydrogenated PAH species in the ISM. Cross-sections for a reaction of a H-atom with PQ and pentacene were derived directly from the experimental data. For the linear catacondensed PAH pentacene, the cross-section is found to be $\sigma = 0.094\ (^{+0.093}_{-0.031})$ Å^2, which is larger than that of the pericondensed PAH coronene studied previously, thereby providing experimental evidence for the difference in reactivity based on the type of edges present in the PAH. For PQ, the cross-section is found to be 0.143 $(^{+0.143}_{-0.048})$ Å^2. This is a factor of 1.5 larger than that of pentacene, thereby providing experimental evidence for the enhanced reactivity of oxygen-functionalised PAHs as compared to their pristine analogues. The higher reaction cross-section of PQ with H-atoms is a possible explanation for why oxygen-functionalised PAHs have not been detected in the gas phase in the ISM. This in turn indicates that oxygen-functionalised PAHs may play a role in the formation of small oxygen-carrying molecules such as OH and H_2O in the ISM via H-abstraction reactions. In the case of PQ, we do not see evidence for smaller carbonaceous fragments that contain an oxygen atom; however, we cannot rule out the formation of such fragments for oxygen-functionalised PAHs with (i) different edge structures (e.g. coronene and corannulene) and (ii) type of oxygen functional group (e.g. C=O, C-OH, C-O-C, etc.). Experiments are underway to investigate the photon-induced gas-phase fragmentation pathways of linear catacondensed oxygen-functionalised PAHs to further understand their role in interstellar chemistry. Future experiments will be focussed on studying the interaction of H- and oxygen atoms with different pristine and oxygen- or nitrogen-functionalised PAHs. In addition, their fragmentation will be studied in detail in the context of the top-down formation of smaller species relevant to prebiotic chemistry.

Acknowledgements. This work has been supported by the E.U. under the Horizon2020 Marie Skłodowska-Curie ITN EUROPAH (Grant agreement no.: 722346) and the Danish National Research Foundation through the Center of Excellence "InterCat" (Grant agreement no.: DNRF150). We also acknowledge financial support from the Danish Council for Independent Research (Grant no.: 5137-00049B), the European Research Council (CoG GRANN, Grant agreement no.: 648551).

References

Allamandola, L. 2011, EAS Pub. Ser., 46, 305
Berné, O., & Tielens, A. G. 2012, Proc. Natl. Acad. Sci., 109, 401
Bernstein, M. P., Sandford, S. A., & Allamandola, L. J. 1996, ApJ, 472, L127
Bernstein, M. P., Sandford, S. A., Allamandola, L. J., et al. 1999, Science, 283, 1135
Bouwman, J., Mattioda, A., Linnartz, H., & Allamandola, L. 2011, A&A, 525, A93
Burkhardt, A. M., Lee, K. L. K., Changala, P. B., et al. 2021, ApJ, 913, L18
Campisi, D., Simonsen, F. D. S., Thrower, J. D., et al. 2020, Phys. Chem. Chem. Phys. 22, 1557
Candian, A., & Sarre, P. 2015, MNRAS, 448, 2960
Cazaux, S., Boschman, L., Rougeau, N., et al. 2016, Sci. Rep., 6, 1
Cazaux, S., Arribard, Y., Egorov, D., et al. 2019, ApJ, 875, 27
Cernicharo, J., Agúndez, M., Cabezas, C., et al. 2021, A&A, 649, L15
Chen, T., Zhen, J., Wang, Y., Linnartz, H., & Tielens, A. G. 2017, Proc. Int. Astron. Union, 13, 353
Cook, A. M., Ricca, A., Mattioda, A. L., et al. 2015, ApJ, 799, 14
De Angelis, F., Gaspari, M., Procopio, A., Cuda, G., & Di Fabrizio, E. 2009, Chem. Phys. Lett., 468, 193
Dulieu, F., Morisset, S., Mohamed, A.-S. I., et al. 2019, Mol. Astrophys., 17, 100054
Fan, G., & Manson, J. 2009, Phys. Rev. B, 79, 045424
Grimmelmann, E. K., Tully, J. C., & Cardillo, M. J. 1980, J. Chem. Phys., 72, 1039
Gudipati, M. S., & Yang, R. 2012, ApJ, 756, L24
Guennoun, Z., Aupetit, C., & Mascetti, J. 2011a, Phys. Chem. Chem. Phys., 13, 7340
Guennoun, Z., Aupetit, C., & Mascetti, J. 2011b, J. Phys. Chem. A, 115, 1844
Habart, E., Boulanger, F., Verstraete, L., & Walmsley, C. 2004, A&A, 414, 531
Ioppolo, S., Fedoseev, G., Lamberts, T., Romanzin, C., & Linnartz, H. 2013, Rev. Sci. Instrum., 84, 073112
Jensen, P. A., Leccese, M., Simonsen, F. D., et al. 2019, MNRAS, 486, 5492
Joblin, C., Tielens, A., Allamandola, L., & Geballe, T. 1996, ApJ, 458, 610
Jurchescu, O. D., Baas, J., & Palstra, T. T. 2004, Appl. Phys. Lett., 84, 3061
Knipp, D., Street, R., Völkel, A., & Ho, J. 2003, J. Appl. Phys., 93, 347
Le Page, V., Snow, T. P., & Bierbaum, V. M. 2009, ApJ, 704, 274
Linstrom, P., & Mallard, W. 2021, NIST Standard Reference Database Number 69 (National Institute of Standards and Technology, Gaithersburg MD, 20899)
Mattioda, A. L., Cruz-Diaz, G. A., Ging, A., et al. 2020, ACS Earth Space Chem., 4, 2227
McGuire, B. A., Burkhardt, A. M., Kalenskii, S., et al. 2018, Science, 359, 202
McGuire, B. A., Loomis, R. A., Burkhardt, A. M., et al. 2021, Science, 371, 1265
Mennella, V., Hornekær, L., Thrower, J., & Accolla, M. 2011, ApJ, 745, L2
Mennella, V., Suhasaria, T., Hornekær, L., Thrower, J., & Mulas, G. 2021, ApJ, 908, L18
Noble, J., Michoulier, E., Aupetit, C., & Mascetti, J. 2020, A&A, 644, A22
Peeters, E., Hony, S., Van Kerckhoven, C., et al. 2002, ApJ, 390, 1089
Peeters, E., Mackie, C., Candian, A., & Tielens, A. G. 2021, Accounts Chem. Res., 54, 1921
Pety, J., Teyssier, D., Fossé, D., et al. 2005, A&A, 435, 885
Rasmussen, J. A. 2013, J. Phys. Chem. A, 117, 4279
Rauls, E., & Hornekær, L. 2008, ApJ, 679, 531
Roberson, L. B., Kowalik, J., Tolbert, L. M., et al. 2005, J. Am. Chem. Soc., 127, 3069
Sadjadi, S., Zhang, Y., & Kwok, S. 2015, ApJ, 807, 95
Salama, F. 2008, Proc. Int. Astron. Union, 4, 357
Simonsen, F. D. S. 2020, PhD thesis, Aarhus University, Denmark
Skov, A. W., Andersen, M., Thrower, J. D., et al. 2016, J. Chem. Phys., 145, 174708
Sloan, G., Bregman, J., Geballe, T., Allamandola, L., & Woodward, E. 1997, ApJ, 474, 735
Thrower, J., Jørgensen, B., Friis, E. E., et al. 2012, ApJ, 752, 3
Tielens, A. G. 2005, The Physics and Chemistry of the Interstellar Medium (Cambridge: Cambridge University Press)
Tielens, A. G. 2008, ARA&A, 46, 289
Tschersich, K. 2000, J. Appl. Phys., 87, 2565
Tschersich, K., & Von Bonin, V. 1998, J. Appl. Phys., 84, 4065
Tschersich, K., Fleischhauer, J., & Schuler, H. 2008, J. Appl. Phys., 104, 034908
Wakelam, V., Bron, E., Cazaux, S., et al. 2017, Mol. Astrophys., 9, 1
Zhen, J., Castellanos, P., Paardekooper, D. M., Linnartz, H., & Tielens, A. G. 2014, ApJ, 797, L30